Journal of Materials Chemistry C

Accepted Manuscript

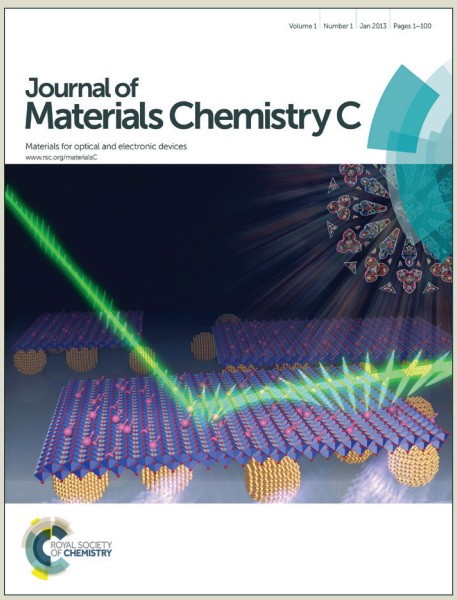

ROYAL SOCIETY OF CHEMISTRY

www.rsc.org/materialsC

Not Your Familiar Two Dimensional Transition Metal Disulfide: Structural and Electronic Properties of PdS_2 Monolayer

Yu Wang,[†], Yafei Li,[†,*] Zhongfang Chen[‡,*]

College of Chemistry and Materials Science, Jiangsu Key Laboratory of Biofunctional Materials, Nanjing Normal University, Nanjing, Jingsu, 210046, China, and Department of Chemistry, Institute for Functional Nanomaterials, University of Puerto Rico, Rio Piedras Campus, San Juan, PR 00931.

To whom correspondence should be addressed. Email: liyafei.abc@gmail.com (YL) and zhongfangchen@gmail.com (ZC)

Abstract

By means of density functional theory (DFT) computations, we theoretically investigated a novel two-dimensional (2D) transition metal disulfide (TMD), namely PdS_2 monolayer. Distinguished from other 2D TMDs which adopt the ordinary 2H or 1T configuration, PdS_2 monolayer presents rather unique structural properties: each Pd atom binds to four S atoms in the same plane, and two neighboring S atoms can form a covalent S–S bond. The hybrid HSE06 DFT computations demonstrated that PdS_2 monolayer is semiconducting with an indirect band gap of 1.60 eV, which can be effectively reduced by employing a uniaxial or biaxial tensile strain. Especially, PdS_2 has a rather large hole and electron mobilities. Our results suggest that PdS_2 monolayer is rather promising for future electronics and optoelectronics.

Introduction

Graphene, which consists of a single layer of sp^2-hybridized carbon atoms arranged in a two-dimensional (2D) honeycomb lattice, was indentified experimentally by Geim and Novoselov in 2004.[1,2] Graphene has fantastic electronic properties, such as mass-less Dirac fermions,[3] room temperature quantum Hall effect,[4] ultrahigh carrier mobility (10^6 cm^2/Vs).[5] Remarkably, graphene also has superb mechanical[6] and thermal[7] properties. These remarkable properties endow graphene many exciting applications in a wide range of fields.[8,9]

The experimental realization of graphene also greatly stimulated the synthesis of 2D structures of inorganic layered materials, such as *h*-BN,[10 – 12] black phosphorus,[13–15] and MAX phases.[16,17] In recent years, 2D transition metal disulfides (TMDs), which consist of one layer of transition metal atoms (TM, typically Mo, W, V, or Ti) sandwiched between two layers of sulfur (S) atoms, have been a subject of extensive studies due to their fantastic properties complementary or even surpassing those of graphene.[18–24] For example, MoS_2 monolayer has a moderate direct band gap (~1.80 eV)[25] as well as a considerable carrier mobility of ~200 cm^2/Vs,[26] rendering it a more suitable candidate for optoelectronics devices and transistors than zero-gap graphene. Depending on the different arrangement of S atoms, 2D TMDs can be roughly divided into two polytypes, one is 2H which consists of trigonal prismatic D_{3h}-TMS_6 units, the other is 1T which consists of octahedral O_h-TMS_6 units. For example, MoS_2 and WS_2 monolayers prefer to adopt the 2H configuration, while the most stable configuration of TiS_2 and SnS_2 monolayers is 1T. Interestingly, the

meta-stable 1T polytype of MoS_2[27,28] and WS_2[29,30] monolayers have also been synthesized recently, which are metallic and show dramatic catalytic performance toward hydrogen evolution.

The pioneering works by Grønvold *et al.*[31–34] demonstrated that some noble metals, such as Pt, and Pd can also form layered structures with S atoms (e. g. PtS_2, PdS_2). Especially, in PdS_2 each Pd atom can only bind to four rather than six S atoms, leading to the formation of rather a novel structure distinguished from other layered TMDs.[35] Inspired by the extensive studies of 2D TMDs, it is expected that PdS_2 can also be exfoliated into monolayer and find some important applications in electronics. Recently, Miró *et al.*[36] theoretically studied the electronic properties of PdS_2 monolayer and found that PdS_2 monolayer is semiconducting. However, they reported that the most stable configuration of PdS_2 monolayer is 1T, which is different from that of the layers in PdS_2 bulk. Considering that the layers in PdS_2 bulk are hold together by weak van der Waals (vdW) interactions, when a PdS_2 monolayer is exfoliated from PdS_2 bulk, it is unlikely that a phase transition occurs, thus we can expect that the exfoliated PdS_2 monolayer should adopt the same configuration as bulk. In this case, a comparison of stability between these possible configurations of PdS_2 monolayer is rather necessary in order to determine the thermodynamically most favorable structure.

In this work, by means of comprehensive density functional theory (DFT) computations, we systematically studied the structural and electronic properties of PdS_2 monolayer. Our results revealed that the most stable configuration of PdS_2

monolayer is neither 1T or 2H, but is featured with planar tetra-coordinate Pd atoms and covalent S–S bonds. PdS_2 monolayer is semiconducting with a moderate indirect band gap and has rather large carrier mobilities, which would endow it many important applications in electronics.

Computational Methods

Our DFT computations were performed using the plane-wave technique implemented in Vienna *ab initio* simulation package (VASP).[37] The ion-electron interaction was described using the projector-augmented plane wave (PAW) approach.[38,39] The generalized gradient approximation (GGA) expressed by PBE functional[40] and a 500 eV cutoff for the plane-wave basis set were adopted in all computations. Especially, for those weak interaction involved computations, the PBE+D2 method with Grimme vdW corrections was adopted.[41] We set the *x* and *y* directions parallel and the *z* direction perpendicular to the basal plane of PdS_2 monolayer, and adopted a supercell length of 25 Å in the *z* direction. The geometry optimizations were performed using the conjugated gradient method, and the convergence threshold was set to be 10^{-5} eV in energy and 10^{-4} eV/Å in force. The Brillouin zone was represented by Monkhorst-Pack special *k*-point mesh of 6×6×1 for geometry optimizations, while larger grid (14×14×1) was used for band structure computations. Since the PBE functional usually underestimates band gaps of semiconductors, in this work all the band structures were computed using the hybrid HSE06 functional[42–44] on the basis of PBE optimized geometric structures. Especially, considering that Pd is a rather heavy element, the spin-orbital coupling (SOC) effect

was also taken into account in band structure computations.

The particle-swarm optimization (PSO) method within the evolutionary scheme as implemented in the CALYPSO code[45] was employed to search the low-energy structures of 2D PdS_2 monolayer. As an unbiased global optimization method, the PSO algorithm was inspired by the choreography of a bird flock and can be viewed as a distributed-behavior algorithm that performs multidimensional search. This method has successfully predicted the low-energy structures of many planar 2D materials.[46–50] A straightforward extension of this method can also be applied to 2D systems with finite thickness. Unit cells of PdS_2 monolayer containing total atoms of 6 and 12 atoms were considered. The structure relaxations during the PSO simulation were performed using the PBE functional, as implemented in VASP.

Results and Discussion

To ascertain the most stable configuration for PdS_2 monolayer, we firstly considered two possible structures, which are displayed in Fig. 1 and named with PdS_2-I and PdS_2-II in the order of increasing total energy. The optimized lattice parameters, bond lengths and relative total energies of two structures are given in Table 1. Both PdS_2-I and PdS_2-II are true local minima as indicated by their all positive phonon modes (Fig. S1, S2). These two structures are also the only stable structures by PSO global search (after 30 generations). We also constructed two other possible configurations, namely 2H and Haeckelite configuration. Following the previous convention of MoS_2, the Haeckelite configuration of PdS_2 monolayer consists of 4-8 defects.[51] However, the 2H configuration is not a local minimum as it

has considerable imaginary phonon modes (Fig. S1), and the Haeckelite configuration of PdS_2 monolayer transforms to PdS_2-I after full geometry optimization. Therefore, only PdS_2-I and PdS_2-II are considered in the following sections.

As shown in Fig. 1, PdS_2-II takes the ordinary 1T configuration, while PdS_2-I can be seen as the monolayer form of PdS_2 bulk and has a rectangular unit cell. Similar to PdS_2-II and other TMD monolayers, PdS_2-I also consists of one Pd atomic layer sandwiched between two S atomic layers. However, different from PdS_2-II in which each Pd atom binds to six S atoms to form an octahedral prismatic, in PdS_2-I each Pd atom is coordinated with four S atoms, and the four Pd–S bonds are in the same plane. Note that the square planar coordination of Pd is also adopted by many common Pd-containing compounds, such as PdO, $PdCl_2$. Especially, in PdS_2-I each S atom can form two Pd–S bonds and one S–S bond with neighboring atoms, whereas in PdS_2-II S atoms can only form Pd–S bonds. More interestingly, in PdS_2-I every two Pd atoms and three S atoms can form a wrinkled pentagon, which is rather rare in known materials. According to our computations, PdS_2-I is 111 meV/atom lower in energy than PdS_2-II, which indicates that PdS_2-I is more stable than PdS_2-II, and thus excludes 1T polytype (PdS_2-II) as the most stable configuration for PdS_2 monolayer. The enhanced stability of PdS_2-I may be due to the presence of covalent S-S bonds.

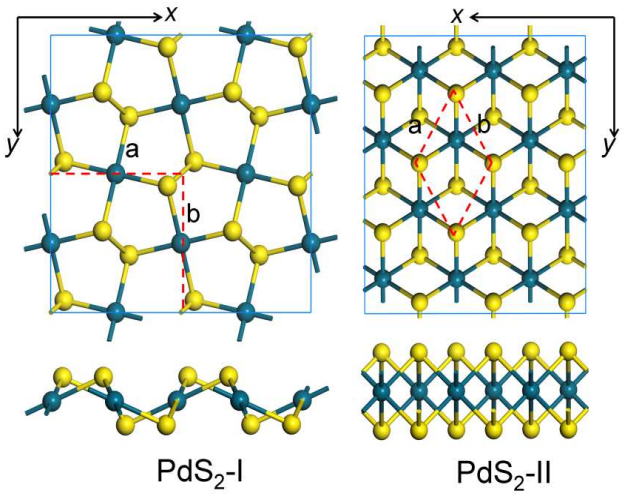

Fig. 1 Top (upper) and side (bottom) views of two structures of PdS_2 monolayer. Black green and yellow balls represent Pd and S atoms, respectively. Both monolayers are extended periodically along the *x* and *y* directions.

Although PdS_2-I is more stable than PdS_2-II, we are still uncertain whether it is the lowest-energy structure for PdS_2 monolayer. To this end, we performed a global search for the lowest-energy structure of PdS_2 monolayer in the whole 2D space using first-principles based particle-swarm optimization (PSO) method as implemented in CALYPSO code. As a benchmark, the PSO method correctly predicted the 2H and 1T configuration as the global minimum structure for MoS_2 and TiS_2 monolayer, respectively, by only one generation search. For PdS_2 monolayer, no structures with lower energy than that of PdS_2-I were found after 30 generations. On the basis of above results, we can safely conclude that PdS_2-I is the most stable configuration for PdS_2 monolayer, and the experimentally realized PdS_2 monolayer would adopt the configuration as that of PdS_2-I. However, the above results don't exclude the possibility of forming 1T-PdS_2. As above mentioned, the meta-stable 1T polytype of

MoS_2 and WS_2 have been realized experimentally,[27-30] thus we can expect that the metal-stable 1T-PdS_2 can also be realized under specific conditions.

Tab. 1 The optimized lattice parameters (*LP*), length of Pd–S ($d_{Pd–S}$) and S–S ($d_{S–S}$) bonds, and relative energy (E_r) of two configurations for PdS_2 monolayer.

Polytype	*LP* (Å)	$d_{Pd–S}$ (Å)	$d_{S–S}$ (Å)	E_r (meV/atom)
PdS_2-I	a = 5.49, b = 5.59	2.34, 2.35	2.10	0
PdS_2-II	a = b = 3.53	2.40	/	110

With so intriguing geometrics, what novel electronic properties can PdS_2 monolayer present? To address this issue, we computed the band structure and density of states (DOS) of the energetically preferred PdS_2 monolayer (PdS_2-I) on the basis of above determined configuration. As shown in Fig. 2, computed at HSE06 theoretical level, PdS_2 monolayer is semiconducting with an indirect band gap of 1.60 eV. The conduction band minimum (CBM) locates at the S (0.5, 0.5, 0) point, while the valence band maximum (VBM) locates in the interval between Γ and X (0.5, 0, 0) points. Remarkably, the direct band gap (1.95 eV) of PdS_2 monolayer is quite close to the indirect band gap, indicating that PdS_2 monolayer would have promising applications in optoelectronics. The partial DOS analysis reveals that the VBM of PdS_2 monolayer is mainly contributed by the S-3*p* states and partially by Pd-4*d* states, while the CBM is contributed by both Pd-4*d* and S-3*p* states with nearly equal weight.

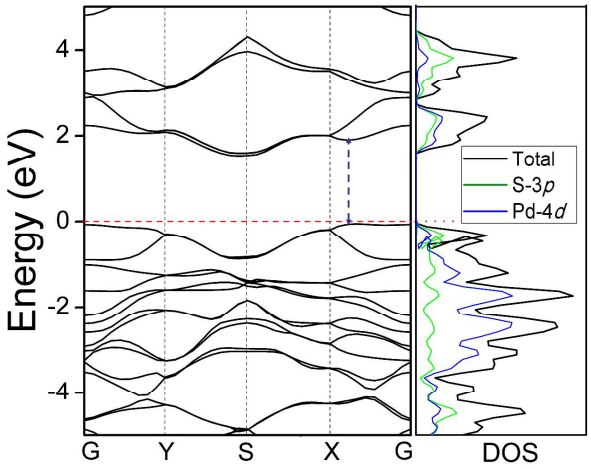

Fig. 2 Band structure (left) and density of states (right) of PdS_2 monolayer. The red dashed line denotes the position of Fermi level while the blue double arrow denotes the direct band gap.

Experimentally, the controllable band gap engineering of nanomaterials is always desirable for wider applications. Applying external elastic strain has proven an efficient method toward tuning the electronic properties of many 2D structures.[52-56] Therefore, we also studied the effect of external strain on the electronic properties of PdS_2 monolayer. We employed both uniaixal and biaxial strains, but only considered the tensile strain as it is more feasible to realize experimentally. Here the strain (ε) is defined as $\varepsilon = (l - l_0) / l_0$, where l and l_0 are the strained and the equilibrium lattice parameters of PdS_2 monolayer, respectively.

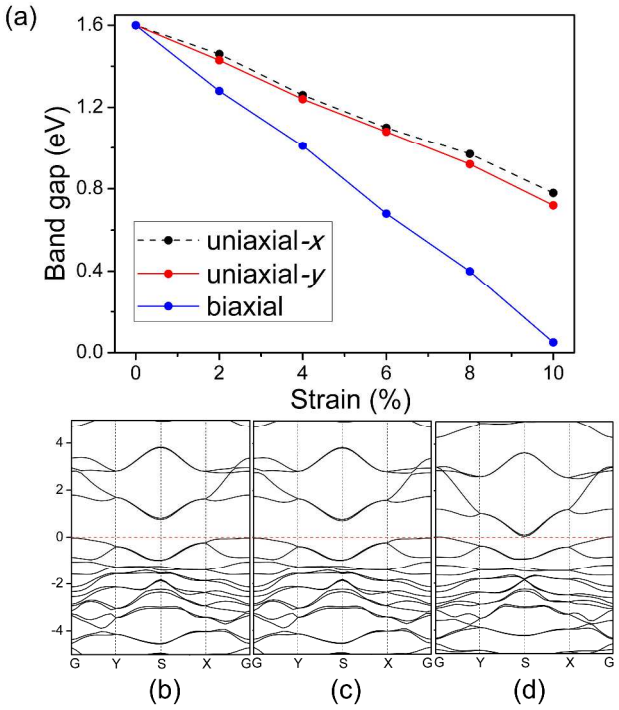

Fig. 3 (a) Plots of band gap versus applied tensile strain for PdS_2 monolayer. (b) and (c) are band structures of PdS_2 monolayer with a uniaxial strain of 10% along the *x* and *y* direction, respectively, whereas (d) is band structure of PdS_2 monolayer with a biaxial strain of 10%.

Our computations demonstrated that the effect of tensile strain on the electronic properties of PdS_2 monolayer is rather pronounced. When subjected to a uniaxial strain, the band gap of PdS_2 decreases monotonically with increasing strain, regardless of the strain direction (Fig. 3a). For example, when the uniaxial strains along the *x* and *y* directions are increased to 10%, the band gaps of PdS_2 monolayer can be reduced to 0.79 and 0.72 eV, respectively. Remarkably, the electronic properties of PdS_2 monolayer are more sensitive to the biaxial strain than the uniaxial strain. With a biaxial tensile strain of 10%, the band gap of PdS_2 monolayer is

significantly reduced to 0.05 eV. It is expected that a semiconducting-metallic transition would be observed with the further increase of tensile strain. The above results indicate that the electronic properties of PdS_2 monolayer can be flexibly modulated by applying an axial tensile strain, which would lead to a wider range of applications.

Besides the band gap, carrier mobility is another important factor for semiconducting materials in devices applications. Recently, it has been shown both experimentally and theoretically that some 2D structures, such MoS_2,[26] and phosphene**Error! Bookmark not defined.**,[14] have a considerable carrier mobility (> 200 $cm^2 V^{-1}s^{-1}$), which makes these materials quite promising candidates for field effect transistors (FET). To obtain more information on the electronic properties of PdS_2 monolayer for future utilization, we investigated its carrier (including electron and hole) mobilities on the basis of deformation potential (DP) theory, which was initially proposed by Bardeen and Shockley.[57] Note that the DP theory has been successfully employed to predict the carrier mobility of many 2D structures.[58–61] According to the DP theory, the carrier mobility (μ) of a 2D structure can be expressed as:

$$\mu = \frac{e\hbar^3 C}{k_B T m^* m_d E_1^2}$$

where $\hbar$ is the reduced Planck constant, k_B is Boltzmann constant, T is the temperature (300 K). C is the in-plane stiffness, which is defined as $C = [\partial^2 E/\partial\varepsilon^2]/l_0$, where E is the total energy of the PdS_2 supercell. m^* is the carrier effective mass along the transport direction (both x and y) and $m_d = \sqrt{m_x^* m_y^*}$ is the average carrier effective mass. E_1 is the deformation potential (DP) constant determine by $E_1 = \partial E_{edge}/\partial\varepsilon$, where E_{edge} is

the value of CBM (for electron) and VBM (for hole). All of these quantities were computed by the HSE06 functional, and the corresponding values are summarized in Table 2.

Tab. 2 The computed effective mass (m^*), in-plane stiffness, deformation potential (E_1), and mobility (μ) of electron and hole along x and y directions for PdS_2 monolayer at 300K.

Carrier type	m^*/m_0	C (N/m)	E_1 (eV)	μ ($cm^2v^{-1}s^{-1}$)
electron (x)	0.87	58	8.59	40.97
electron (y)	0.25	82	9.40	169.11
hole (x)	0.72	58	2.12	339.25
hole (y)	1.75	82	3.11	91.73

According to our computations, the m^* of electron and hole for PdS_2 monolayer along the x direction are 0.87 m_0 and 0.72 m_0 (m_0 is the free electron mass), respectively, whereas those along the y direction are 0.25 m_0 and 1.75 m_0, respectively. Our computations also revealed that PdS_2 monolayer has anisotropic mechanical properties: the in-plane stiffness are 58 N/m and 82 N/m along the x and y directions, respectively. As a comparison, the in-plane stiffness of MoS_2 monolayer is ~128 N/m,[60] indicating that PdS_2 is much softer than MoS_2 monolayer. By fitting the band edge-strain curves (Fig. 4), we found that the deformation potential (E_1) of hole are rather small, namely 2.12 (x direction) and 3.11 (y direction), respectively, whereas E_1 of electron are rather large, taking the respective values of 8.59 (x direction) and 9.40 (y direction). On the basis of the obtained m^*, C, and E_1, the acoustic phonon-limited carrier mobilities were then computed. The mobilities of electron are 40.97 (x

direction) and 149.11 cm^2/Vs (y direction), respectively. Remarkably, due to the rather small deformation potential (E_1), the mobilities of hole are much larger than those of electron, with a value of 339.25 (x direction) and 91.73 (y direction) cm^2/Vs, respectively. Especially, the mobilities of both hole and electron for PdS_2 monolayer are larger than those of MoS_2 monolayer.[60] Therefore, PdS_2 monolayer would be a quite promising material for future applications in electronic and optoelectronic devices.

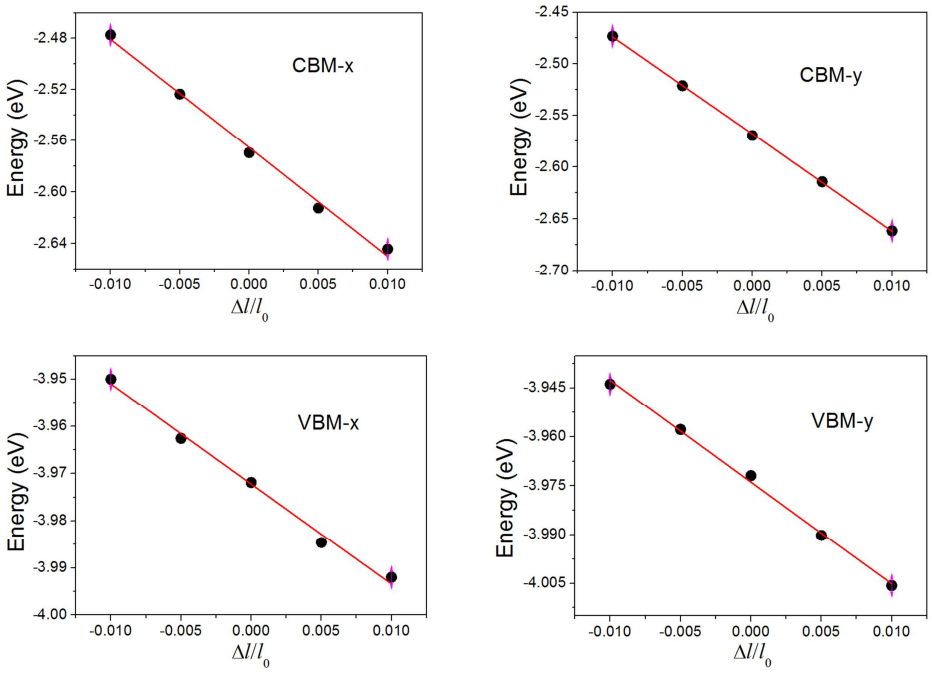

Fig. 4 Shifts of CBM and VBM under uniaxial strain along x and y directions for PdS_2 monolayer. Δl refers to the dilation along x or y, while l_0 refers to the lattice constant of a or b at equilibrium geometry.

After revealing the structural and electronic properties of PdS_2 monolayer, we quite wonder whether this novel 2D structure can be realized experimentally. To

address this question, we computed the interlayer binding energy (E_b) of PdS_2 bulk and compared to some known layered materials to evaluate the feasibility of exfoliating one PdS_2 monolayer from PdS_2 bulk. According to our results, the E_b per unit cell of PdS_2 is 855 meV, which is much higher than those of graphite (209 meV), *h*-BN (280 meV), and black phosphorus (607 meV). However, we should note that the unit cell area of PdS_2 is much larger than those of graphite, *h*-BN, and black phosphorus, and the strength of vdW interaction has a close relationship with the interface area. In this case, the average binding energy of PdS_2 (27.88 meV/Å^2) is actually much lower than those of graphite (39.89 meV/Å^2), *h*-BN (52.14 meV/Å^2), and black phosphorus (39.93 meV/Å^2). As graphene, *h*-BN monolayer, and phosphene have been realized experimentally by exfoliation or epitaxial growth, it is expected that PdS_2 monolayer can be realized via similar methods.

Conclusion

In this work, we theoretically investigated the structural and electronic properties of a novel 2D material, namely PdS_2 monolayer by means of DFT computations. Distinguished from common 2D TMDs, PdS_2 monolayer has the rather unique structural properties featured with planar tetracoordinate Pd atoms and S-S bonds. PdS_2 monolayer is semiconducting with an indirect band gap of 1.60 eV and a quite close direct band gap of 1.95 eV. The electronic properties of PdS_2 monolayer can be effectively modulated by applying the tensile strain. Especially, PdS_2 monolayer has rather high carrier mobilities. The above properties render PdS_2 monolayer a promising candidate for future electronics. Considering the rapid development of

experimental techniques for fabricating 2D materials, e. g. $PtSe_2$ monolayer,[62] PdS_2 monolayer would be realized experimentally soon.

Moreover, other noble-transition-metal dichalcogenides may also not take the ordinary 1T and 2H configurations, our test computations showed that $PdSe_2$ monolayer can take the same configuration as that of PdS_2 monolayer, while the 1T configurations is favored by $PdTe_2$ monolayer and Pt dichalcogenides (PtS_2, $PtSe_2$, $PtTe_2$) monolayers (Table 3). The different structural properties of Pd dichalcogenides from those of Pt dichalcogenides may be due to the differences in electronegativity and atomic radius between Pd and Pt. We hope that our studies can stimulate more efforts on exploring the structural and electronic properties of novel 2D materials.

Tab. 3 Optimized lattice parameters and relative energies for PdS_2-type and 1T configurations of $PdSe_2$, $PdTe_2$, PtS_2, $PtSe_2$, and $PtTe_2$ monolayers. For each monolayer, the enengy of 1T configuration was set as zero.

Monolayer	**Configuration**	***LP* (Å)**	**E_r (meV/atom)**
$PdSe_2$	PtS_2-type	a = 5.74, b = 5.92	–25
	1T	a = b = 3.74	0
$PdTe_2$	PtS_2-type	a = 5.99, b = 6.37	15
	1T	a = b = 4.03	0
PtS_2	PtS_2-type	a = 5.47, b = 5.56	45
	1T	a = b = 3.58	0
$PtSe_2$	PtS_2-type	a = 5.73, b = 5.91	102
	1T	a = b = 3.75	0
$PtTe_2$	PtS_2-type	a = 5.97, b = 6.35	113
	1T	a = b = 4.02	0

Supporting Information. Phonon spectrum of PdS_2 monolayer in the most stable configuration, 1T configuration, and 2H configuration. This material is available free of charge via the Internet at http://pubs.rsc.org.

Acknowledgement. Support in China by NSFC (21403115) and Priority Academic Program Development of Jiangsu Higher Education Institutions, and in USA by Department of Defense (Grant W911NF-12-1-0083) and National Science Foundation (Grant EPS-1010094) is gratefully acknowledged. The computational resources utilized in this research were provided by Shanghai Supercomputer Center.

References

[1] K. S. Novoselov, A. K. Geim, S. V. Morozov, D. Jiang, Y. Zhang, S. V. Dubonos, I. V. Gregorieva and A. A. Firsov, *Science*, 2004, **306**, 666.

[2] K. S. Novoselov, D. Jiang, F. Schedin, T. J. Booth, V. V. Khotkevich, S. V. Morozov and A. K. Geim, *Proc. Natl. Acad. Sci. U.S.A.*, 2005, **102**, 10451.

[3] K. S. Novoselov, A. K. Geim, S. V. Morozov, D. Jiang, I. V. Khotkevich, I. V. Gregorieva, S. V. Dubonos and A. A. Firsov, *Nature*, 2005, **438**, 197.

[4] K. S. Novoselov, Z. Jiang, Y. Zhang, S. V. Morozov, H. L. Stormer, U. Zeitler, J. C. Maan, G. S. Boebinger, P. Kim and A. K. Geim, *Science*, 2007, **315**, 1379.

[5] K. Kim, J. Y. Choi, T. Kim, S. H. Cho, H. J. Chung, *Nature*, **2011**, *479*, 338.

[6] C. G. Lee, X. D. Wei, J. W. Kysar and J. Hone, *Science*, 2008, **321**, 385.

[7] A. A. Balandin, S. Ghosh, W. Bao, I. Calizo, D. Teweldebrhan, F. Miao and C. N. Lau, *Nano Lett*., 2008, **8**, 902.

[8] K. S. Novoselov, V. I. Falko, L. Colombo, P. R. Gellert, M. G. Schwab and P. Kim, *Nature*, 2012, **490**, 192.

[9] V. Georgakilas, M. Otyepka, A. B. Bourlinos, V. Chandra, N. Kim, K. C. Kemp, P. Hobza, R. Zboril and K. S. Kim, *Chem. Rev*., 2012, **112**, 6156.

[10] C. Y. Zhi, Y. Bando, C. C. Tang, H. Kuwahara and D. Golberg, *Adv. Mater*., 2009, **21**, 2889.

[11] J. H. Warner, M. H. Rümmeli, A. Bachmatiuk and B. Büchner, *ACS Nano*, 2010, **4**, 1299.

[12] A. Nag, K. Raidongia, K. P. S. S. Hembram, R. Datta, U. V. Waghmare and C. N. R. Rao, *ACS Nano*, 2010, **4**, 1539.

[13] L. Li, Y. Yu, G. J. Ye, Q. Ge, X. Ou, H. Wu, D. Feng, X. H. Chen and Y. Zhang, *Nat. Nanotechnol.*, 2014, **9**, 372.

[14] H. Liu, A. T. Neal, Z. Zhu, D. Tomanek and P. D. Ye, *ACS Nano*, **2014**, *8*, 4033.

[15] F. Xia, H. Wang and Y. Jia, *Nat. Commun*., 2014, **5**,4458.

[16] M. Naguib, O. Mashtalir, J. Carle, V. Presser, J. Lu, L. Hultman, Y. Gogotsi and M. W. Brrsoum, *ACS Nano*, 2012, **6**, 1322.

[17] O. Mashtalir, M. Naguib, V. N. Mochalin, Y. Dall'Angese, M. Heon, M. W. Barsoum and Y. Gogotsi, *Nat. Commun*., 2013, **4**, 1716.

[18] Q. H. Wang, K. Kalantar-Zadeh, A. Kis, J. N. Coleman and M. S. Strano, *Nat. Nanotechnol.*, 2012, **7**, 699.

[19] S. Z. Butler, S. M. Hollen, L. Cao, Y. Cui, J. A. Gupta, H. R. Gutiérrez, T. F. Heinz, S. S. Hong, J. Huang, A. F. Ismach, E. Johnston-Halperin, M. Kuno, V. V. Plashnitsa, R. Robinson, R. S. Ruoff, S. Salahuddin, J. Shan, L. Shi, M. G. Spencer, M. Torrones, W. Windl and J. E. Goldberger, *ACS Nano*, 2013, **7**, 2898.

[20] M. S. Xu, T. Liang, M. Shi and H. Chen, *Chem. Rev.*, **2013**, **113**, 3766.

[21] M. Chhowalla, H. S. Shin, G. Eda, L. -J. Li, K. P. Loh and H. Zhang, *Nat. Chem.*, 2013, **5**, 263.

[22] A. Kuc and T. Heine, *Chem. Soc. Rev.*, 2015, DOI: 10.1039/C4CS00276H.

[23] T. Heine, *Acc. Chem. Res.*, 2015, **48**, 65.

[24] P. Miró, M. Audiffred and T. Heine, *Chem. Soc. Rev.*, 2014, **43**, 6537.

[25] K. F. Mak, C. Lee, J. Hone, J. Shan and T. F. Heinz, *Phys. Rev. Lett.*, 2010, **105**, 136805.

[26] B. Radisavljevic, A. Radenovic, J. Brivio, V. Giacometti and A. Kis, *Nat. Nanotechnol.*, 2011, **6**, 147.

[27] D. Voiry, M. Salehi, R. Silva, T. Fujita, M. Chen, T. Asefa, V. B. Shenoy, G. Eda and M. Chhowalla, *Nano. Lett.*, 2013, **12**, 6222.

[28] M. A. Lukowski, A. S. Daniel, F. Meng, A. Forticaux, L. Li and S. Jin, *J. Am. Chem. Soc.*, 2013, **135**, 10274.

[29] D. Voiry, H. Yamaguchi, J. Li, R. Silva, D. C. Alves, T. Fujita, M. Chen, T. Asefa, V. B. Shenoy, G. Eda and M. Chhowalla, *Nat. Mater.*, 2013, **12**, 850.

[30] M. A. Lukowski, A. S. Daniel, C. R. English, F. Meng, A. Forticaux, R. J. Hamers and S. Jin, Energy Environ. Sci., 2014, **7**, 2608.

[31] F. Grønvold and R. Røst, *Acta Chem. Scand.*, 1956, **10**, 1620.

[32] A. Kjekshus and F. Grønvold, *Acta Chem. Scand.*, 1959, **13**, 1767.

[33] F. Grønvold, H. Haraldsen and A. Kjekshus, *Acta Chem. Scand.*, 1960, **14**, 1879.

[34] F. Grønvold and R. Røst, *Acta Cryst.*, 1957, **10**, 329.

[35] C. Soulard, X. Rocquefelte, P.-E. Petit, M. Evain, S. Jobic, J.-P. Itie, P. Munsch, H.-J. Koo and M.-H. Whangbo, *Inorg. Chem.*, 2004, **43**, 1943.

[36] P. Miró, M. Ghorbani-Asl and T. Heine, *Angew. Chem. Int. Ed.*, 2014, **53**, 3015.

[37] G. Kresse and J. Hafner, *Phys. Rev. B*, 1993, **47**, 558.

[38] P. E. Blöchl and *Phys. Rev. B*, 1994, **50**, 17953.

[39] G. Kresse and D. Joubert, *Phys. Rev. B*, 1999, **59**, 1758.

[40] J. P. Perdew, L. Burke and M. Ernzerhof, *Phys. Rev. Lett.*, 1996, **77**, 3865.

[41] W. Reckien, F. Jantzko, M. Peintinger and T. Bredow, *J. Comput. Chem.*, 2012, **33**, 2023.

[42] J. Heyd, G. E. Scuseria and M. Ernzerhof, *J. Chem. Phys*., 2003, **118**, 8207.

[43] J. Heyd, G. E. Scuseria and M. Ernzerhof, *J. Chem. Phys*., 2006, **124**, 219906.

[44] V. Barone, O. Hod, J. E. Peralta and G. E. Scuseria, *Acc. Chem. Res.*, 2011, **44**, 269.

[45] Y. Wang, J. Lv, L. Zhu and Y. Ma, *Phys. Rev. B*, 2010, **82**, 094116.

[46] X. Luo, J. Yang, H. Liu, X. Wu, Y. Wang, Y. Ma, S. H. Wei, X. Gong and H. Xiang, *J. Am. Chem. Soc.*, 2011, **133**, 16285.

[47] J. Dai, Y. Zhao, X. J. Wu, J. L. Yang and X. C. Zeng, *J. Phys. Chem. Lett.*, 2013, **4**, 561.

[48] X. J. Wu, J. Dai, Y. Zhao, Z. W. Zhuo, J. L. Yang and X. C. Zeng, *ACS Nano*, 2012, **6**, 7443.

[49] Y. Li, Y. Liao and Z. Chen, *Angew. Chem. Int. Ed*., 2014, **53**, 7248.

[50] Y. Li, Y. Liao, P. v. R. Schleyer and Z. Chen, *Nanoscale*, 2014, **6**, 10784.

[51] H. Terrones and M. Terrones, 2D Materials, *2014*, **1**, 011003.

[52] K. He, C. Poole, K. F. Mak and J. Shan, *Nano Lett.*, 2013, **13**, 2931.

[53] Y. Y. Hui, X. Liu, W. Jie, N. Y. Chan, J. Hao, Y. T. Hsu, L. J. Li, W. Guo and S. P. Lau, *ACS Nano*, 2013, **7**, 7126.

[54] A. Castellanos-Gomez, R. Roldán, E. Cappelluti, M. Buscema, F. Guinea, H. S. J. van der Zant and G. A. Steele, *Nano Lett.*, 2013, **13**, 5361.

[55] S. Zhang, Z. Yan, Y. Li, Z. Chen and H. Zeng, *Angew. Chem. Int. Ed*., 2015, **54**, 3112.

[56] Y. Li and Z. Chen, *J. Phys. Chem. C*, 2014, **118**, 1148.

[57] J. Bardeen and W. Shockley, *Phys. Rev*., 1950, **80**, 72.

[58] M. Long, L. Tang, D. Wang, L. Wang and Z. Shuai, *J. Am. Chem. Soc.*, 2009, **131**, 17728.

[59] M. Long, L. Tang, D. Wang, Y. Li and Z. Shuai, *ACS Nano*, 2011, **5**, 2593.

[60] Y. Cai, G. Zhang and Y. –W. Zhang, *J. Am. Chem. Soc.*, 2014, **136**, 6269.

[61] J. Qiao, X. Kong, Z. -X. Hu, F. Yang and W. Ji, *Nat. Commun*., 2014, **5**, 4475.

[62] Y. Wang, L. Li, W. Yao, S. Song, J. T. Sun, J. Pan, X. Ren, C. Li, E. Okunishi, Y. Wang, E. Wang, Y. Shao, Y. Y. Zhang, H. Yang, E. F. Schwier, H. Iwasawa, K. Shimada, M. Taniguchi, Z. Cheng, S. Zhou, S. Du, S. J. Pennycook, S. T. Pantelider, H. J. Gao. *Nano. Lett*. 2015, **15**, 4013.

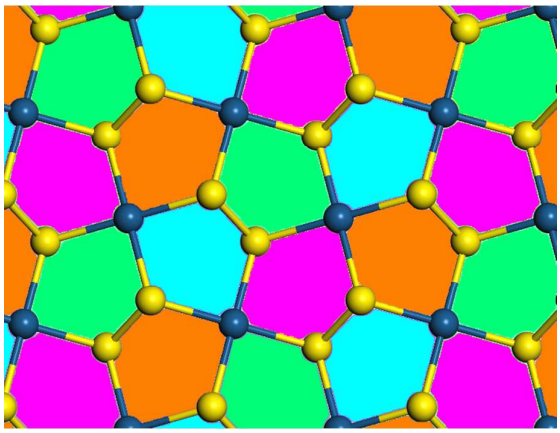

PdS_2 monolayer has distinguished strucutral properties from other transistion metal disulfides, and has also ranther high carrier mobilities. It is semiconducting with a moderate indirect band gap, which could be effectively tuned by applying a tensile strain.